Metal Oxide Nanocrystals - Review

L.Vijay
I Year- MECH
St.Anne's College of Engineering and Technology
Panruti

A. John Peter
Asst.professor
Department of Physics
St.Anne's College Of Engineering and Technology
Panruti

S. Masilla Moses Kennedy
Asst.professor,
Department of Physics
SSN College of Engineering Old Mahabalipuram Road
SSN Nagar, Kalavakkam

Abstract **- Size effects constitute a fascinating aspect of nanomaterials. As the size of a crystal decreases to the nanometer regime, the associated properties are increasingly governed by considerations such as the surface-area-to-volume ratio and energy quantization. Quantum confinement is a widely used terminology in the study of nanocrystals. Size quantization refers to changes in the energy-level structures of materials as the building unit size drops below a certain size. This size, which can be identified with the Bohr diameter of the material, can vary from almost 100 nm to a single nanometer or even less. The electronic structure is altered from the continuous electronic bands to discrete or quantized electronic levels leading to the size-dependent properties. Further since the properties of nanocrystals follow from the confinement of the electrons to the physical dimensions of the nanocrystals, it would be interesting to vary the shape of the nanocrystals, study on the effect of confinement of electrons in such artificial shapes, and follow by optimizing the physiochemical properties.**

Keywords: Nano crystals, luminescence, quantum confinement and phosphors.

1. INTRODUCTION

Within the broad family of functional materials, metal oxides play a very important role in many scientific and technological areas. For decades they have been extensively investigated for their physiochemical properties and useful applications by solid-state chemists. Oxides including the transition metals and rare earths, display a very wide variety of complex structures and interesting properties. These metal elements are able to form a large diversity of oxide compounds, giving the inspiration for designing new materials. The crystal structures are often fabricated by the formation of the metal-oxygen bonds to produce simple rock salt or complex oxide with varying nearly ionic to covalent or metallic. The oxidic materials exhibit fascinating electronic and magnetic properties associating with the changes in electronic structure and bonding. Additionally, metal oxides having multivalent oxidation states have attracted much attention among specialists because they often exhibit superior catalytic reaction performance.

2 TYPES OF METAL OXIDE NANOCRYSTALS

2.1. Transition metal oxides

Transition metal oxides generally show ordered defect complexes or extended defects instead of isolated point defects (Rawls 1981). They also occur as shear structures or infinitely adaptive structures. Some structure types such as rock salt, spinel, rutile, cuprite, fluorite, and corundum type structures, play an important role in the identification of their complex structures (Corpuz and Richards 2010). A variety of transition metal oxides exhibits transformations from one crystal structure to another as the temperature or pressure is varied. The phase transformations of their crystal structure often undergo the changes of the atomic, electronic or spin configuration. Transition metal oxides include both localized and itinerant *d*-electron behavior (Thiel 1998). Typical examples of transition metal monoxides are MnO, CoO, and NiO, processing the rock salt structure. The cation *d* orbitals in the rock salt structure would be splitted into t_2g and e_g sets by the octahedral crystal field of the anions. While in transition metal monoxide, TiO and NiO ($3d^2$ and $3d^8$), the *d* levels would be partially filled; hence the simple band theory predicts them to be metallic. The prediction is true in the case of TiO and to some extent in the case of VO. Stoichiometric MnO, CoO, NiO are, however, all good insulators showing

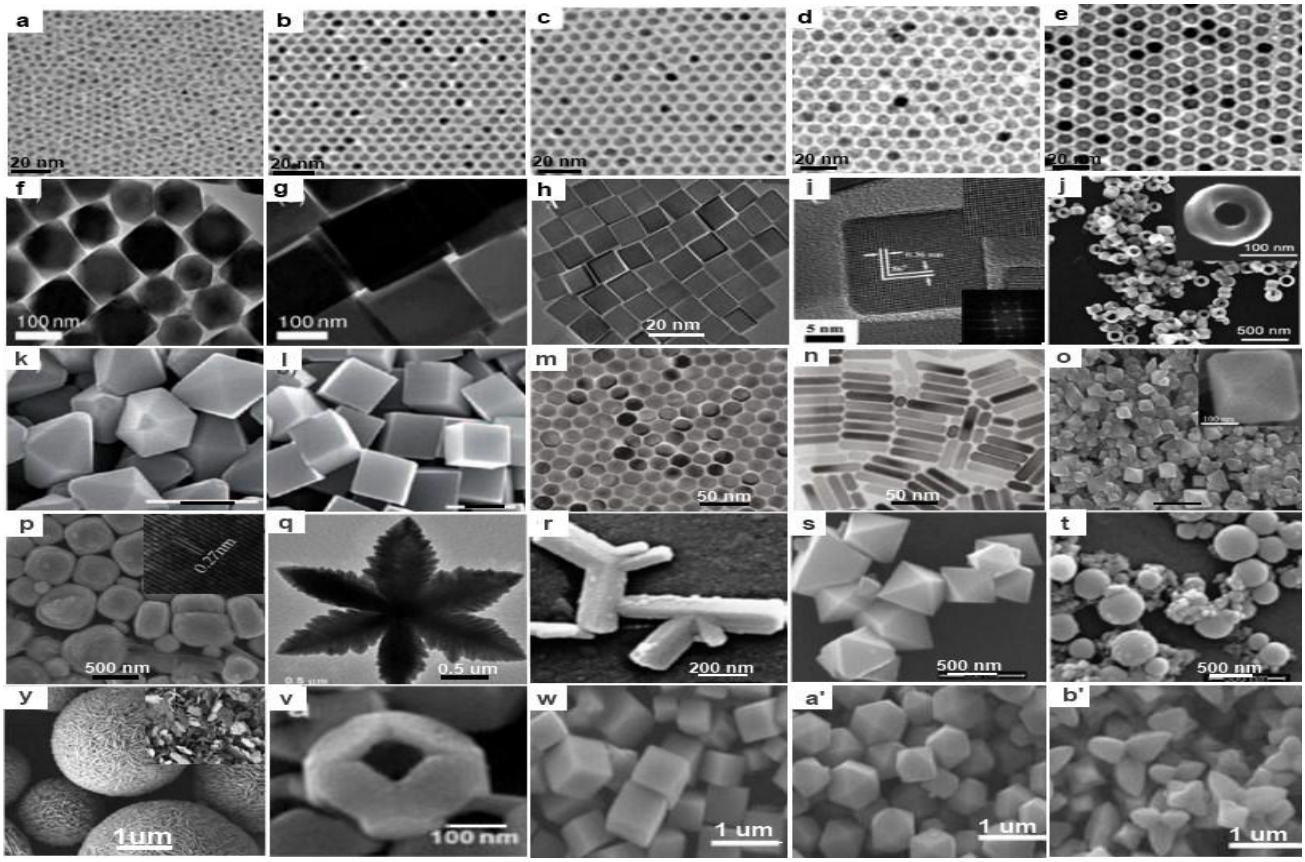

Figure 2.1. Gallery of representative TEM/HRTEM/SEM images of synthesized transition-metal oxide nanocrystals. Monodisperse iron oxide nanospheres with controlled particle sizes of (a) 6 nm, (b) 8 nm, (c) 10 nm, (d) 11 nm, (e) 13 nm(Park et al. 2005); (f) mixture of truncated cubic and truncated octahedral nanocrystals and (g) truncated nanocubes of Fe_3O_4 species (Park et al. 2005); (h,i) pseudocubic iron oxide nanocrystals, inset FFT pattern (Wang and Gao 2009); (j) single-crystalline alpha-Fe_2O_3 nanorings (Jia et al. 2008); single-crystalline iron oxide nanocrystals with (k) tetrakaidecahedron and (l) oblique parallelepiped shapes (Wang et al. 2010a); Mn_3O_4 nanocrystals with (m) spherical and (n) rod shapes and (o) $LiMn_2O_4$ nanocrystals (Wang et al. 2010c); (p) nest-like SnO nanostructures (Ning et al. 2009); (q) alpha-Fe_2O_3 nanosnowflakes, (r) Mn_2O_3 triangular nanorods, (s) CoO octahedral nanostructures, and (t) Cr_2O_3 nanospheres (Polshettiwar, Baruwati and Varma 2009); (y) hollow Cu_2O microspheres (Zhang et al. 2007a); (v) Cu_2O.

antiferromagnetism. The insulating nature of FeO can be understood by assuming that the t_{2g} subband is completely filled for the $3d^6$ configuration, but the insulating nature of MnO, CoO, NiO cannot be understood in terms of simple band theory (Baerends Evert, Gritsenko Oleg and van Leeuwen 1996).

Transition metal oxide nanocrystals are particularly useful in various applications in magnetic field (Mahmoudi et al. 2010). The synthesis of well-defined magnetic nanocrystals is an important issue, because magnetic properties change drastically with particle size. Representative TEM/HRTEM//SEM examples of a variety of transition metal oxide nanocrystals are shown in Figure 2-1. The hot injection and heat-up processes are generally carried out in hot surfactant solutions and have been widely used to synthesize uniform nanocrystals. Iron carbonyl, acetate, acetylacetonate, carboxylate, and chloride are some of the commonly used precursors for making monodisperse iron oxide nanocrystals. For example, the thermal decomposition of $Fe(CO)_5$ in octyl ether in the presence of oleic acid or lauric acid resulted in the formation of essentially amorphous iron particles (Hyeon et al. 2001). Spherical alpha-Fe_2O_3 nanocrystals could also be directly generated with size ranging from 4 to 16 nm by introducing an oxidation agent, trimethylamine *N*-oxide or $(CH_3)_3NO$, into the reaction solution. Hyeon et al.(Park et al. 2005) revealed that monodisperse iron nanoparticles with different sizes of 4, 8, 11 nm were prepared by changing the molar $Fe(CO)_5$:oleic acid ratio from 1:1 to 1:2 and 1:3. In a next step, these seed nanocrystals were reacted with iron oleate solutions of defined concentrations, resulting in monodisperse iron nanocrystals that transform into iron oxide nanoparticles of 6, 7, 8, 9, 10, 11, 12, 13 nm on exposure to air (Figure 2-5a-e). Cheon et al.(Cheon et al. 2004) had achieved the thermal decomposition of $Fe(CO)_5$ in *o*-dichlorobenzene/dodecylamine to yield alpha-Fe_2O_3 nanocrystals with controlled different shapes, including diamonds (40%), triangle plates (30%), and spheres (30%). Zeng et al.(Sun and Zeng 2002) reported the synthesis of

monodisperse magnetite nanoparticles from iron(III) acetylacetonate, $Fe(acac)_3$, using a high-temperature reaction. In this approach, 4 nm magnetite nanoparticles were formed by refluxing a reaction mixture composed of $Fe(acac)_3$, diphenyl ether, 1,2-hexadecanediol, oleic acid, and oleylamine. A seeded growth process was also demonstrated for generating large nanoparticles. By controlling the ratio of seed relative to the precursor, nanoparticles up to 16 nm in diameter were obtained. Using different precursors, including $Fe(acac)_3$, iron acetate, O'Brien et al.(Redl et al. 2004) had explored the thermal decomposition of iron pentacarbonyl in trioctylamine or octyl ether in the presence of oxidants such as pyridine *N*-oxide and trimethyl *N*-oxide hydrate to wüstite Fe*x*O ($0.84 < x < 0.95$) nanocrystals. Some recent progresses for the controlled synthesis of high-quality transition metal oxide nanocrystals were achieved. The representative examples of iron oxide nanocrystals are illustrated. Gao et al. (Wang and Gao 2009) reported the morphology-controlled synthesis and magnetic property of pseudocubic iron oxide nanoparticles using the mixture of iron(III) chloride/sodium oleate/oleic acid/ethanol. Lu et al.(Wang et al. 2010a) synthesized the single-crystalline iron oxide nanocrystals with tetrakaidecahedron and oblique parallelepiped shapes and high-index facets exposed in high yields through the solvothermal reaction of a mixture of $K_3[Fe(CN)_6]$, N_2H_4, sodium carboxymethyl cellulose at 160 ^oC for 6 h. Magnetic properties of these two kinds of nanocrystals displayed shape-dependent magnetic behaviors. Raabe et al.(Jia et al. 2008) presented a novel approach for synthesizing single-crystalline alpha-Fe_2O_3 nanorings with outer diameters of 150-170 nm, inner diameters of 70-100 nm, and heights of 80-120 nm, employing a double anion-assisted hydrothermal treatment of the aqueous solution of $FeCl_3$, $NH_4H_2PO_4$, Na_2SO_4 at 220 °C for 48 h. Gao et al.(Wang and Gao 2009) have prepared alpha-Fe_2O_3 nanoparticles enclosed by six (Burda et al.) of planes, in which the uniformity of morphology should be further improved. Yan et al.(Jia et al. 2005a) reported on the synthesis of single-crystalline alpha-Fe_2O_3 nanotubes through a coordination assisted dissolution process involving the selective adsorption of phosphate ions on hematite. Zeng et al.(Xu and Zeng 2004) synthesized Co_3O_4 nanocubes smaller than 10 nm and their superstructures by adding capping agent Tween-85 into their reaction system.

Considerable effort has been devoted to the development of alternative energy storage/conversion devices with high power and energy densities because of the up-coming depletion of fossil fuels. Recent progress has been devoted to synthesis and electrochemical applications for oxide nanomaterials. For example, the solvothermal reaction of $Mn(NO_3)_2$/oleylamine/dodecanol recently flourished by Li et al.(Wang et al. 2010c) was a successful way for shape control of highly monodisperse Mn_3O_4 nanocrystals with dot, rod wire shapes. Moreover, the as-prepared hydrophobic spherical or elongated nanoparticles were used as building blocks to be rationally assembled into three-dimensional (3D) Mn_3O_4 colloidal spheres with a facile ultrasonication route. The as-prepared colloidal spheres were chemically converted to $LiMn_2O_4$ nanomaterials in a simple solid-state reaction. Such materials showed distinct electrochemical performance, mainly depending on their crystallinity and particle size. Dai et al.(Wang et al. 2010d) reported a two-step solution-phase method for growing Mn_3O_4 nanoparticles on graphene oxide to form a Mn_3O_4-reduced graphene oxide hybrid material. The grown of Mn_3O_4 nanoparticles on graphene oxide sheets includes two steps: (i) hydrolysis of $Mn(CH_3COO)_2$ in a graphene oxide suspension with a 10:1 *N*,*N*-dimethylformamide (DMF)/H_2O mixed solvent at 80 °C, (ii) distribution of well-crystallized Mn_3O_4 nanoparticles on graphene oxide sheets by transferring the above reaction solution to deionized water and treated in hydrothermal conditions at 180 °C for 10 h. The gas-liquid interfacial route was used to synthesize water-soluble Fe_3O_4 nanoparticles in iron nitrate, ethylene glycol (EG) and ammonia solution. The Fe_3O_4 nanoparticles could be incorporated into a carbon matrix under the hydrothermal method and such materials exhibited excellent anode materials for high-performance Li^+-ion batteries (Cui et al. 2009b). The vanadium pentoxide (V_2O_5) has been attracting much attention in low-cost energy battery because it can serve as the anode in Li ion battery design or as the cathode material in rechargeable Li ion batteries.

2.2 Rare earth oxides

The chemically similar fourteen elements in the bottom of periodic table ranging in atomic number from 57 to 71 are known as the lanthanoids that have in common an open 4*f* shell. The lanthanides are sometimes referred to as the "rare earths" which originates from the isolation of these elements early in their discovery (Greinacher 1981). The lanthanide ions are trivalent and their physiochemical properties principally originate from the trivalent ions which are important rather than those of the neutral atoms. A series of lanthanide thus possesses many similar chemical and physical properties to the other members of the lanthanoid group. It is noted that lanthanum should be considered a member of the lanthanide family as it lacks *f*-electrons (Le roy and Holmberg 1963). The Group III transition metals Sc and Y are also frequently included in discussions about the lanthanides due to having many similar properties to the lanthanide family of elements. The electron configuration of the lanthanides range from [Xe] $6s^25d^1$ for lanthanum (La) to [Xe] $6s^24f^{14}5d^1$ for lutetium (Lu). The 4f orbitals lie well inside the electronic shell and are well protected from external influences by the filled 6*s* and 5*p* orbitals. Although the trend is observed from the atomic radii, it is best shown by the radii of the trivalent cations. A consequence of the lanthanide contraction is that holmium (Ho^{3+}) is the same size as the much lighter Y^{3+} with corresponding similar properties. The majority of the optical properties of the lanthanide ions can also be attributed to the shielded nature of the 4*f* orbitals (Moeller 1967).

Recently, high-quality rare-earth nanocrystals have drawn great attention because of their unique physical and chemical properties and potential applications in the fields

of catalysis, luminescence devices, optical transmission, biochemical probes, medical diagnostics, and so forth (Shen, Sun and Yan 2008, Zhang et al. 2010a). The different synthetic routes have been developed to a number of size- and shape-controlled dispersible rare earth oxide nanocrystals. Representative TEM//HRTEM/SEM examples of a variety of rare earth oxide nanocrystals are shown in Figure 2-5. Yan et al.(Si et al. 2005) synthesized the single-crystalline and monodisperse cubic rare-earth (RE = La to Lu, Y) oxide nanocrystals with plate and disk shapes via a nonhydrolytic approach in oleic acid/oleylamine/1-octadecene using various rare-earth complexes, including acetylacetonate, benzoylacetonate, and acetate, as the precursors. The selective adsorption of coordinating oleic acid ligands onto specific crystal planes of cubic RE_2O_3 nanocrystals made them adopt a plate shape with the confined growth of facets and/or a disk shape with the confined growth of facets. The as-prepared high-quality luminescent Y_2O_3:Eu ultrathin nanodisks displayed strong surface-dependent, highly pure red emissions that were due to selective incorporation of Eu^{3+} ions in the surface of the nanodisks (Si et al. 2006). The hydrolysis of metal nitrates in octadecylamine to generate the rare earth (Ce) and transition (Ni, Zn, Co) oxide nanocrystals was achieved by Li et al.(Wang et al. 2008a). Subsequently, calcination was carried out to remove the surfactants to produce mesoporous metal oxides by surfactant-assisted self-assembly process, which showed large pores thermally stable pore mesostructures, and potential applications in catalysis and lithium-ion batteries. By thermolysis of rare-earth benzoylacetonate complexes in oleic acid/oleylamine, Xu et al.(Zhang et al. 2007d) synthesized the Y_2O_3:Tb nanorods were obtained by self-assembly of long-chain alkyl amine-capped nanocrystals prepared from thermolysis of yttrium-oleate complexes.

Gao et al.(Yang and Gao 2006) reported the shape- and size-controlled synthesis of uniform CeO_2 nanocubes by reaction of cerium nitrate aqueous solution and *tert*-butylamine in toluene/oleic acid at 180 °C via a solvo-hydrothermal two-phase process. Adschiri et al.(Zhang et al. 2007b) modified this reaction system for the synthesis of CeO_2 nanocubes using cerium hydroxide precursors under supercritical water conditions. The product shape could be controlled by tuning the interaction of organic molecules with various crystallographic planes of fluorite cubic ceria. The morphology and displayed crystallite plane of CeO_2 nanocrystals could be controlled by the length of dicarboxylic acids (Taguchi et al. 2009). The ceria nanocrystals with spherical, wire, and tadpole shapes were controllably fabricated via a nonhydrolytic sol-gel process using oleic acid and oleylamine as cosurfactant (Yu et al. 2005b).

Very recently, Si et al.(Du et al. 2007b) synthesized ceria nanocrystals via an alcohothermal process at 180 °C in ethanol, using alkylamine as the base and polyvinylpyrrolidone as the stabilizer, and furthermore, the ceria nanocrystals were self-organized into chainlike and dendritic nanostructures by oriented attachment. Xia el al.(Yu et al. 2010) recently synthesized the CeO_2 nanosheets with lateral dimensions up to 4 μm and thickness of ~2.2 nm by the heating of the aqueous cerium nitrate solution in the presence of 6-aminohexanoic acid ligand. Yan et al.(Zhou et al. 2008) reported a rapid thermolysis of $(NH_4)_2Ce(NO_3)_6$ in oleic acid/oleylamine to generate the CeO_2 nanoflowers from the aggregation of tiny particle by a unique 3D oriented-attachment mechanism due to a well-maintained balance of the nucleation and growth stages. The CO catalytic performance of CeO_2 nanocatalysts with different shapes were illustrated. For CO conversion to CO_2 from 200 to 400 ^oC, the activity of the catalysts followed the trend of nanoflowers > nanopolyhedra > nanocubes, in good agreement with the order of the specific surface areas. This result indicated that the flower-shaped catalyst with higher specific surface area could provide more active sites for CO conversion.

Pure ZrO_2 can exist in three polymorphs at atmospheric pressure, e.g., monoclinic (*m*, between room temperature and 1170 °C), tetragonal (*t*, between 1170 and 2370 °C), and cubic (*c*, between 2370 and 2706 °C) phases (Srinivasan et al. 1993, Rashad and Baioumy 2008). Tang et al.(Tang et al. 2008) reported one-step controllable synthesis for ultrafine ZrO_2 nanocrystals via a two-phase interface hydrolysis reaction under hydrothermal conditions. The coexisting *m*- and *t*-ZrO_2 nanocrystals can be found under this condition.

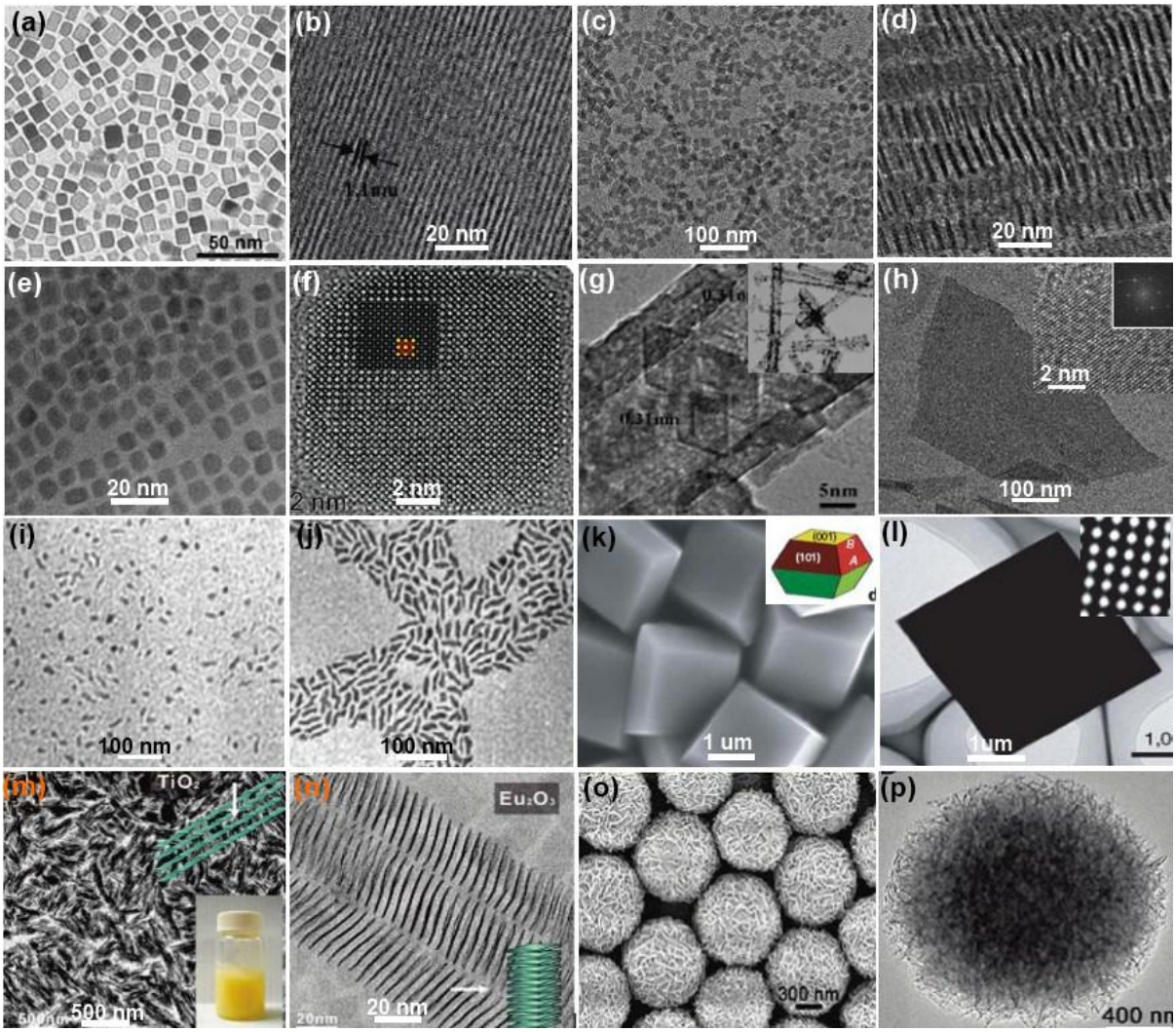

Figure 2.2. Gallery of representative TEM/HRTEM/SEM images of transition-metal oxide nanocrystals: (a) CeO_2 nanocubes (Wang et al. 2008a); Sm_2O_3 with (b) wire, (c) square, (d) plate shapes (Yu et al. 2006); (e,f) CeO_2 nanocubes (Yang and Gao 2006); (g) CeO_2 nanotubes (Zhou, Yang and Yang 2007); (h) CeO_2 nanosheets (Yu, Lim and Xia 2010); (i,j) ZrO_2 nanorices (Zhao et al. 2006); (k,l) single-crystalline truncated TiO_2 nanocrystals (Yang et al. 2008); (m) TiO_2 rod-shaped superstructures, inset of an image of the as-prepared gel-like product; (n) Eu_2O_3 nanodisks (Huo et al. 2009); (o,p) TiO_2 microspheres (Chen et al. 2010a).

Zhao et al.(Zhao et al. 2006) reported the mixed *m*- and *t*-ZrO_2 nanocrystals synthesized via a two-phase approach. Lin et al.(Lin, Zhang and Lin 2007) reported the mixed *m*- and *t*-ZrO_2 nanocrystals synthesized via the pechini-type sol-gel process. Becker et al.(Becker et al. 2008, Zheng et al. 2009) reported mixed *m*- and *t*-ZrO_2 nanocrystals synthesized in near- and supercritical water and supercritical isopropyl alcohol. The phase stability of nanocrystalline ZrO_2 depends upon the size, e.g., the critical size is 10 nm. The tetragonal ZrO2 and monoclinic ZrO_2 can coexist between 11 and 30 nm, while pure monoclinic ZrO_2 is stable with the size above approximately 30 nm. Becker et al. (Bremholm, Becker-Christensen and Iversen 2009) regarded that the critical particle size stems from the difference in the surface energy of the two ZrO_2 polymorphs, with *t*-ZrO_2 being lowest. The structure of nanomaterials surfaces contributes significantly to the energetic character of nanomaterials. The nonhydrolytic sol-gel reaction between zirconium(IV) isopropoxide and zirconium(IV) chloride at 340 °C to generate large quantities of highly monodisperse tetragonal zirconia nanocrystals (~4 nm) were performed by Hyeon et al.(Joo et al. 2003).

CONCLUSION:

Nanostructured metal oxide materials have been the focus of intense research by chemists and materials scientists in various fields due to both their unique properties and technological applications (Seshadri 2005, Burda et al. 2005, Mao et al. 2007, Yin and Alivisatos 2005). Metal oxides including the transition metals and rare earths, display a wide variety of complex structures and interesting electronic and magnetic properties associated with the changes in electronic structure and bonding and in the presence of ordered defect complexes or extended defects.

Furthermore, the size- and shape-dependent properties of nanomaterials raising expectations for a better performance generally are a consequence of quantum confinement within the particle (Alivisatos 1996).

REFERENCES

[1] Abbet, S. & U. Heiz. 2005. Nanocatalysis. Wiley-VCH Verlag GmbH & Co. KGaA.
[2] Alivisatos, A. P. (1996) Semiconductor Clusters, Nanocrystals, and Quantum Dots. Science, 271, 933-937.
[3] Bigioni, T. P., X.-M. Lin, T. T. Nguyen, E. I. Corwin, T. A. Witten & H. M. Jaeger (2006) Kinetically driven self assembly of highly ordered nanoparticle monolayers. Nat Mater, 5, 265-270.
[4] Burda, C., X. Chen, R. Narayanan & M. A. El-Sayed (2005) Chemistry and Properties of Nanocrystals of Different Shapes. Chemical Reviews, 105, 1025-1102.
[5] Cushing, B. L., V. L. Kolesnichenko & C. J. O'Connor (2004) Recent Advances in the Liquid-Phase Syntheses of Inorganic Nanoparticles. Chemical Reviews, 104, 3893-3946.
[6] Jun, Y.-w., J.-s. Choi & J. Cheon (2006) Shape Control of Semiconductor and Metal Oxide Nanocrystals through Nonhydrolytic Colloidal Routes. Angewandte Chemie International Edition, 45, 3414-3439.
[7] Kamat, P. V., K. Tvrdy, D. R. Baker & J. G. Radich (2010) Beyond Photovoltaics: Semiconductor Nanoarchitectures for Liquid-Junction Solar Cells. Chemical Reviews, 110, 6664-6688.
[8] Kinge, S., M. Crego-Calama & D. N. Reinhoudt (2008) Self-Assembling Nanoparticles at Surfaces and Interfaces. ChemPhysChem, 9, 20-42.
[9] Kroes, G.-J., A. Gross, E.-J. Baerends, M. Scheffler & D. A. McCormack (2002) Quantum Theory of Dissociative Chemisorption on Metal Surfaces. Accounts of Chemical Research, 35, 193-200.
[10] MalenfantPatrick, R. L., J. Wan, S. T. Taylor & M. Manoharan (2007) Self-assembly of an organic-inorganic block copolymer for nano-ordered ceramics. Nat Nano, 2, 43-46.
[11] Mao, Y., T.-J. Park, F. Zhang, H. Zhou & S. S. Wong (2007) Environmentally Friendly Methodologies of Nanostructure Synthesis. Small, 3, 1122-1139.
[12] Moores, A. & F. Goettmann (2006) The plasmon band in noble metal nanoparticles: an introduction to theory and applications. New Journal of Chemistry, 30, 1121-1132.
[13] Na, H. B., I. C. Song & T. Hyeon (2009) Inorganic Nanoparticles for MRI Contrast Agents. Advanced Materials, 21, 2133-2148.
[14] Nagarajan, R. 2008. Nanoparticles: Building Blocks for Nanotechnology. In Nanoparticles: Synthesis, Stabilization, Passivation, and Functionalization, 2-14. American Chemical Society.
[15] Park, J., J. Joo, S. G. Kwon, Y. Jang & T. Hyeon (2007) Synthesis of Monodisperse Spherical Nanocrystals. Angewandte Chemie International Edition, 46, 4630-4660.
[16] Rao, C. N. R., A. Müller & A. K. Cheetham. 2005. Nanomaterials – An Introduction. Wiley-VCH Verlag GmbH & Co. KGaA.
[17] Redl, F. X., K. S. Cho, C. B. Murray & S. O'Brien (2003) Three-dimensional binary superlattices of magnetic nanocrystals and semiconductor quantum dots. Nature, 423, 968-971.
[18] Schmid, G. 2005. General Introduction. Wiley-VCH Verlag GmbH & Co. KGaA.
[19] Sellinger, A., P. M. Weiss, A. Nguyen, Y. Lu, R. A. Assink, W. Gong & C. J. Brinker (1998) Continuous self-assembly of
[20] Organic-inorganic nanocomposite coatings that mimic nacre. Nature, 394, 256-260.
[21] Seshadri, R. 2005. Oxide Nanoparticles. Wiley-VCH Verlag GmbH & Co. KGaA.
[22] Shopsowitz, K. E., H. Qi, W. Y. Hamad & M. J. MacLachlan (2010) Free-standing mesoporous silica films with tunable chiral nematic structures. Nature, 468, 422-425.
[23] Sorensen, C. M. 2009. Particles as Molecules. John Wiley & Sons, Inc.
[24] Yin, Y. & A. P. Alivisatos (2005) Colloidal nanocrystal synthesis and the organic-inorganic interface. Nature, 437, 664-670.
[25] Ying, J. Y. (2000) Nanostructural tailoring: Opportunities for molecular engineering in catalysis. AIChE Journal, 46, 1902-1906.
[26] Zhang, H., E. W. Edwards, D. Wang & H. Mohwald (2006) Directing the self-assembly of nanocrystals beyond colloidal crystallization. Physical Chemistry Chemical Physics, 8, 3288-3299.